Effect of Trap States on Interfacial Electron Transfer between Molecular Absorbates and Semiconductor Nanoparticles

Encai Hao,† Neil A. Anderson, John B. Asbury, and Tianquan Lian*

Department of Chemistry, Emory University, Atlanta, Georgia 30322

Received: May 16, 2002; In Final Form: July 17, 2002

TiO_2 and ZrO_2 nanocrystals synthesized by the thermal decomposition of molecular precursors in hot surfactant solvents show much improved crystallinity compared with nanoparticles prepared via hydrolysis of metal alkoxides in water (Trentler, T. J.; Denler, T. E.; Bertone, J. F.; Agrawal, A.; Colvin, V. L. *J. Am. Chem. Soc.* **1999**, *121*, 1613). In this work, we examine the effect of crystallinity and therefore the trap-state density on the dynamics of interfacial electron transfer between adsorbates and nanoparticles. Subpicosecond mid-IR and visible transient absorption spectroscopic techniques were used to study electron-injection and recombination dynamics of TiO_2 and ZrO_2 nanoparticles and nanocrystalline thin films sensitized with catechol and coumarin-343. Comparison of dynamics in materials with different crystallinity demonstrates that electron recombination dynamics are strongly dependent on the preparation method, and the effect on injection dynamics is significant when the injection energy level is near the conduction band edge.

Introduction

Great interest in nanocrystalline metal oxides, particularly TiO_2, has been generated because of their applications in solar energy conversion[1−3] and photocatalysis.[4−6] As a result, the dynamics of interfacial electron transfer in colloidal semiconductor nanoparticles and thin films have recently been the subjects of intensive study.[7−35] The colloidal metal oxide nanoparticles examined in these studies are usually prepared by the hydrolysis of metal alkoxides or halides in water (henceforth, we will refer to these as nanoparticles, NPs).[36−38] NPs prepared using these methods have fully hydroxylated surfaces and a high density of defect states.[38] Interfacial electron-transfer dynamics in these particles were shown to be affected by chemical modification of surface trap states.[14−16,39]

Recent developments in the synthesis of inorganic nanocrystals using rapid thermal decomposition of molecular precursors in hot organic surfactants have produced markedly improved nanoparticles (henceforth, we will refer to these as nanocrystals, NCs).[40] Recently, TiO_2[41] and γ-Fe_2O_3[42] NCs have been prepared successfully using this technique. The resulting TiO_2 nanocrystals have nonhydroxylated surfaces that are capped by trioctylphosphine oxide (TOPO) ligands. These particles show high crystallinity, as indicated by transmission electron microscopy images and powder X-ray diffraction patterns.[41] It is expected that these metal oxide NCs possess fewer surface trap states, which may lead to different interfacial electron-transfer properties compared with those of colloidal nanoparticles prepared via the hydrolytic route.[41]

In this paper, we compare the interfacial electron transfer (ET) dynamics in nanocrystals prepared by high-temperature synthesis in organic surfactants with those in nanoparticles prepared using low-temperature hydrolysis. Specifically, interfacial ET dynamics were examined in coumarin-343 (C-343)-sensitized TiO_2 and ZrO_2 NCs as well as in catechol-sensitized TiO_2 NCs. The observed ET dynamics are compared with those in the corresponding NP systems and nanocrystalline thin films. Subpicosecond transient absorption spectroscopy using mid-IR and visible probes was used to monitor electron injection from the molecular adsorbates to the semiconductor and subsequent back electron transfer. Significant differences in electron-injection, back electron transfer, and electron-trapping dynamics were observed between NCs, NPs, and thin films. These differences are explained in the context of the different crystallinity and density of trap states of the materials.

Experimental Section

Sample Preparation and Characterization. TiO_2 and ZrO_2 NCs were prepared by nonhydrolytic solution-based reactions using the procedure published by Trentler and co-workers.[41] Briefly, 0.44 mL of $TiCl_4$ was mixed with 5.0 g of trioctylphosphine oxide (TOPO) in heptadecane (24 mL) and heated to 270 °C under dry nitrogen. Titanium (IV) isopropoxide (1.19 mL) was rapidly injected into the hot solution. Reactions were completed in 5 min. TiO_2 NCs were then precipitated by the addition of reagent-grade acetone and redispersed in heptane. ZrO_2 NCs were prepared using $ZrCl_4$ and the zirconium(IV) isopropoxide−2-propanol complex as precursors. A longer reaction time (1.5 h) and a higher temperature (>300 °C) were needed. TiO_2 and ZrO_2 NPs were prepared by the hydrolysis of metal alkoxides in water.[36,37] C-343 and catechol-sensitized TiO_2 and ZrO_2 NPs were also prepared according to published procedures.[22,43]

To prepare C-343-sensitized TiO_2 nanocrystals, a fine powder of C-343 dye was mixed with TiO_2/heptane solution and sonicated for 45 min. The mixed solution was then filtered to produce a clear TiO_2/C-343 solution. Because C-343 is not soluble in neat heptane, the C-343 molecules dissolved into TiO_2/heptane solution are believed to adsorb onto the TiO_2 NCs. This assumption is further supported by the observation that C-343 solubility increases in solutions containing higher TiO_2 concentrations. C-343-sensitized ZrO_2 was prepared using the same method. For TiO_2/catechol samples, TiO_2 NCs were

* Corresponding author. E-mail: tlian@emory.edu.
† Current address: Department of Chemistry, Northwestern University, Evanston, Illinois 60208.

10.1021/jp021226m CCC: $22.00
Published on Web 09/07/2002

dissolved in DMF, into which catechol powder was dissolved using an ultrasonicator. The colorless solution quickly changed to red because of the formation of charge-transfer complexes.[39,43] On the basis of these results, both C-343 and catechol can displace the TOPO ligand that caps the surface of TiO_2 and ZrO_2 NCs.

TiO_2 nanocrystalline thin films were prepared by a method similar to that used by Zaban and co-workers.[44] Briefly, the TiO_2 nanoparticle colloid was synthesized by the controlled hydrolysis of titanium(IV) isopropoxide in a mixture of glacial acetic acid and water at 0 °C. The resulting solution was heated to 80 °C for 8 h and was then autoclaved at 230 °C for 12 h. The resulting colloid was concentrated to 150 g/L, spread onto polished sapphire windows, and baked at 400 °C for 36 min. The ZrO_2 nanocrystalline thin films were prepared by a method previously described[2] using ZrO_2 nanoparticles obtained from Degussa Corporation. The films were dipped into a solution of C-343 in ethanol to allow the adsorption of dyes and were then rinsed with ethanol. The sensitized films were stored in a pH 2 aqueous solution.

Powder X-ray diffraction patterns (XRD) of NCs and NPs were examined using molybdenum X-rays and an APEX CCD detector. Transmission electron microscopy (TEM) images were taken with a JEOL 1210 TEM operated at 100 kV. To prepare TEM samples, a few drops of the NC-containing heptane solution was added to water to form a thin-film layer on the surface. Carbon-coated copper grids (200 mesh) were allowed to float on the organic film for 1 min, after which these grids were dried under ambient conditions. Care was taken to avoid deposition of the film on both sides of the grid.

Femtosecond Pump/Probe Measurements. The femtosecond infrared spectrometer used for the time-resolved electron-transfer dynamics study is based on an amplified 1-kHz femtosecond Ti/sapphire laser system and nonlinear frequency-mixing techniques. The details of the experimental setup have been described elsewhere.[7,11,14] All samples were excited at 400 nm. Signals arising from electrons injected into the semiconductor were detected by probing in the mid-IR from 1900 to 2050 cm^{-1}. For catechol-sensitized TiO_2 samples, a series of visible probe wavelengths from 430 to 590 nm were also collected to investigate the behavior of the adsorbates. During transient absorption measurements, the sample solutions flowed through a Harrick IR cell or were scanned rapidly to avoid permanent photoproduct build up on the cell windows. UV−visible absorption spectra collected before and after the measurement showed no noticeable sample degradation.

Results

Figure 1 shows the TEM image of ZrO_2 NCs prepared by the thermal decomposition of $ZrCl_4$ and the zirconium(IV) isopropoxide−2-propanol complex in hot surfactant. The ZrO_2 particles are well dispersed on the carbon-coated grid. The particles exhibit a uniform size distribution with an average diameter of 3 nm. TiO_2 NCs had a larger size distribution and an average diameter of ∼7 nm, consistent with the published results.[41]

Figure 2 shows the XRD patterns of TiO_2 NCs and TiO_2 NPs. Peak positions and relative peak intensities are given in Tables 1 and 2. Both TiO_2 NCs and TiO_2 NPs have the anatase structure. The NC sample shows sharper diffraction peaks than the NP sample, which is attributed to better crystallinity in TiO_2 NCs.

TiO_2/Catechol Charge-Transfer Complexes. Figure 3 shows the absorption spectrum of the catechol/TiO_2 NC in DMF. Also shown for comparison is the spectrum of the unsensitized TiO_2 NC in DMF. The catechol/TiO_2 NC solution exhibits a broad absorption band in the visible region that is not present in catechol or TiO_2 alone. This absorption band has a peak near

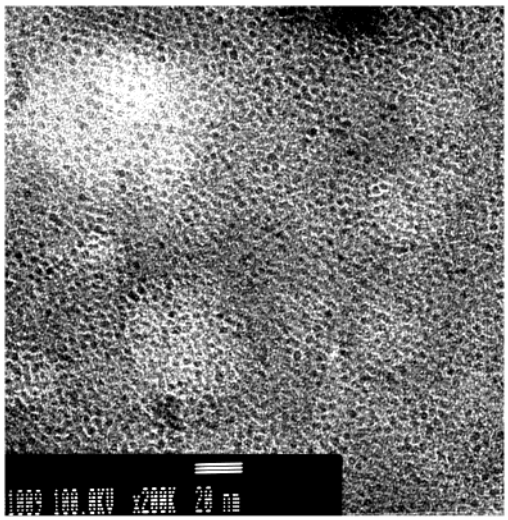

Figure 1. Transmission electron micrograph of ZrO_2 NCs.

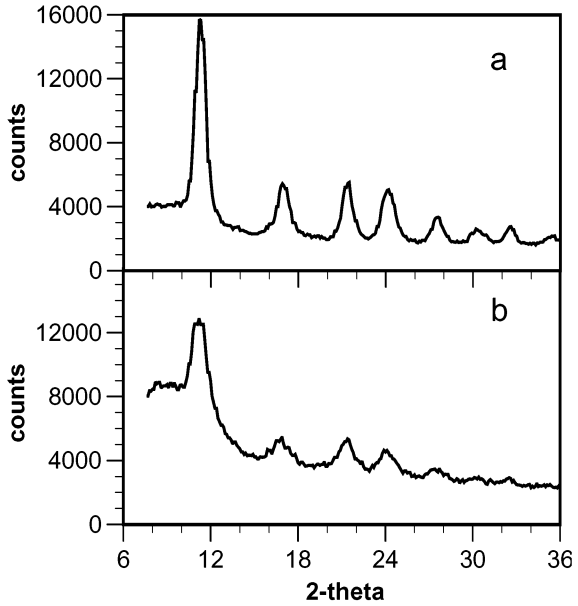

Figure 2. Powder X-ray diffraction patterns of (a) TiO_2 NCs and (b) TiO_2 NPs.

TABLE 1: Powder X-ray Diffraction (XRD) of TiO_2 NCs

2θ angle	intensity	d spacing (Å)	card vol (anatase)
11.434	100	3.567	3.51
17.126	50	2.387	2.379
21.566	40	1.899	1.891
24.198	50	1.695	1.695
27.689	20	1.485	1.480
30.170	10	1.365	1.367
32.779	10	1.259	1.264
35.585	5	1.163	1.161

TABLE 2: Powder X-ray Diffraction (XRD) of TiO_2 NPs

2θ angle	intensity	d spacing (Å)	card vol (anatase)
11.305	100	3.61	3.51
17.004	30	2.400	2.379
21.332	30	1.92	1.891
24.311	20	1.688	1.695
27.587	10	1.491	1.494

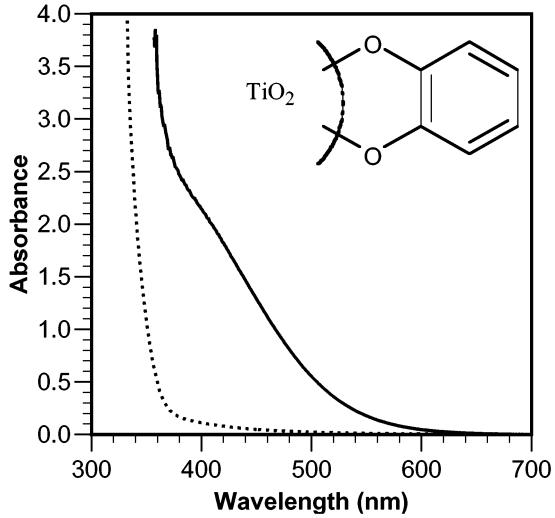

Figure 3. UV−visible absorption spectra of TiO_2 NCs (· · ·) and catechol-sensitized TiO_2 NCs (—) in DMF solution. A schematic structure of the catechol/TiO_2 complex is also shown.

420 nm and a tail extending to 600 nm. A similar absorption band was also observed in the catechol/TiO_2 NP and has been assigned to a catechol-to-titanium charge-transfer (CT) transition.[39,43]

Recently, femtosecond infrared spectroscopy has been successfully used to study interfacial electron transfer between dyes and semiconductor NPs.[10,14,15,22] Monitoring the mid-IR absorption of electrons in the semiconductor allows the direct measurement of electron-transfer dynamics. Transient absorption traces for catechol/TiO_2 complexes were collected by probing in the 2000 cm^{-1} region after the photoexcitation of the charge-transfer band at 400 nm. Figure 4 shows the kinetic traces at 2000 cm^{-1} for sensitized TiO_2 NCs (frame A) and NPs (frame B). Both samples exhibit a fast (<100 fs time scale) absorption increase attributable to electron injection into the semiconductor. The catechol/TiO_2 NC absorption signal decays on time scales of ∼180 ps and ≫1 ns. The catechol/TiO_2 NP signal decays much more quickly, with very little residual absorption remaining at 1 ns.

In adsorbate-to-nanoparticle charge-transfer complexes, photoexcitation leads to direct charge separation, creating electrons in the nanoparticles and oxidizing the adsorbates. The observed <100 fs rise of the electron absorption signal in TiO_2, shown in Figure 4, is consistent with the direct excitation of the charge-transfer band. The total IR absorption signal of the injected electrons, $S(t)$, depends on the electron population, $N(t)$ and the absorption cross section, $\sigma(t)$:[14,15]

$$S(t) = N(t)\,\sigma(t) \qquad (1)$$

The decay of the mid-IR signal can come from population decay due to back electron transfer (back ET) and electron-absorption cross-section decay caused by trapping or relaxation within the semiconductor conduction band and trap states.[14,15] The dynamics of these two processes can be separated if either the back ET or the electron cross-section decay can be determined independently.

To measure the back ET dynamics directly, the recovery of the catechol-to-titanium charge-transfer band in catechol was also studied. The behavior of this band is independent of electron-trapping processes in the semiconductor. Traces at a series of probe wavelengths ranging from 430 to 590 nm were collected for both NP and NC samples. A photobleach of the charge-transfer band was seen at wavelengths below 490 nm. The normalized 450-nm probe traces are shown in Figure 4 for both samples. All probe wavelengths from 430 to 490 nm showed similar dynamics. The bleach recovers more quickly for catechol/TiO_2 NPs, indicating faster back ET dynamics in that sample.

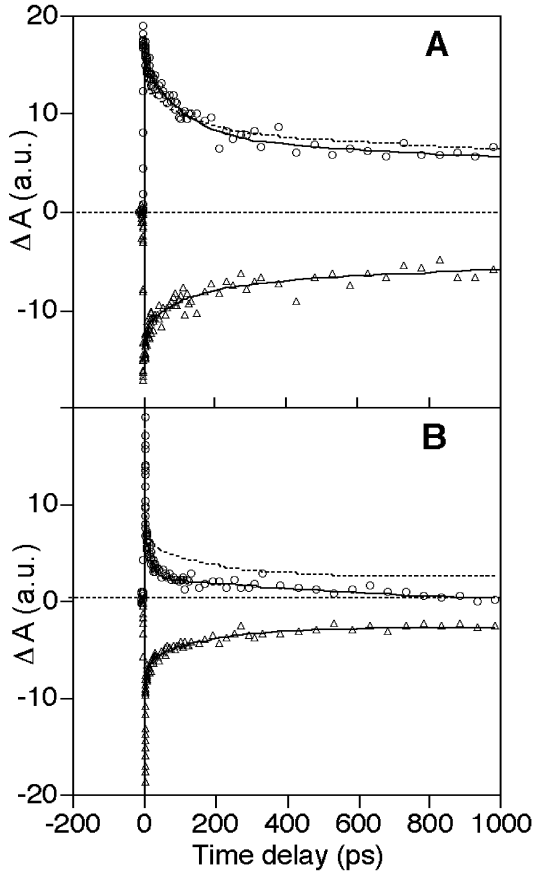

Figure 4. (A) Transient absorption data for catechol/TiO_2 NCs probing the injected electron signal at 2000 cm^{-1}(○) and the CT bleach at 450 nm (△). The dotted line is a projection of the 450-nm fit onto the IR absorption (inverted and scaled). (B) Equivalent data for catechol/TiO_2 NPs.

In Figure 4, the fit lines for the 450-nm traces have been inverted and projected onto the IR absorption signals to allow a clear comparison of the visible (CT band) and IR (injected electron) dynamics in both samples to be made. In the catechol/TiO_2 NC sample, the CT bleach and injected electron absorption signals exhibit similar dynamics, indicating that electron cross-section decay is negligible. This is not the case for the NP sample, where the electron signal clearly decays more quickly than the ground-state bleach recovery, showing that there is significant cross-section decay. According to eq 1, the electron cross section can be calculated by dividing the total IR absorption signal by the population of electrons, which is proportional to the magnitude of the bleach.[14] The calculated electron cross-section decay is presented in Figure 5. The electron cross section in NCs shows only ∼10% decay within 500 ps, whereas that in the NPs shows ∼50% decay in the same time period.

C-343-Sensitized TiO_2 and ZrO_2. To investigate the effects of nanoparticle preparation on electron-injection dynamics, C-343-sensitized NCs and NPs of TiO_2 and ZrO_2 were studied. ET dynamics in C-343/TiO_2 NPs have been previously published.[22] The absorption spectrum of C-343-sensitized TiO_2 NCs in heptane is shown in Figure 6. Also shown for comparison

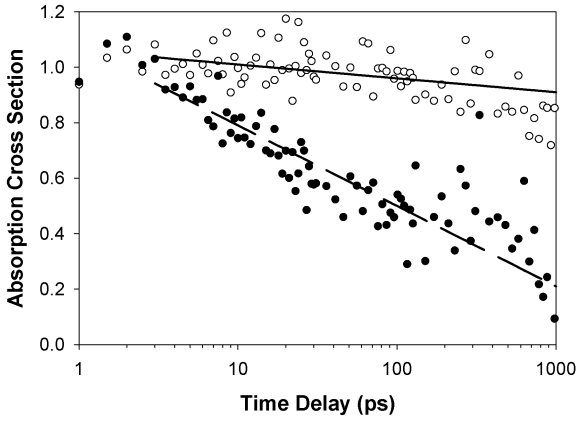

Figure 5. Normalized electron IR absorption cross-section decay in TiO_2 NCs (○) and NPs (●). The cross section is calculated by dividing the electron IR absorption signal for catechol/TiO_2 at 2000 cm^{-1} by its population (magnitude of the bleach at 450 nm).

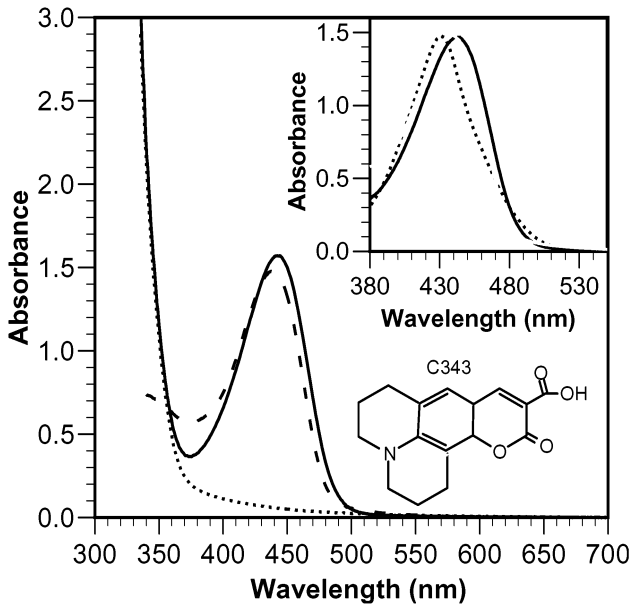

Figure 6. UV−visible absorption spectra of TiO_2 NCs in heptane (• • •), C-343 in ethanol (− − −), and C-343-sensitized TiO_2 NCs in heptane (—). A schematic structure of C-343 is also shown. The inset shows a comparison of the absorption spectra of C-343-sensitized TiO_2 (—) and ZrO_2(• • •) NCs in heptane.

are absorption spectra of TiO_2 NCs in heptane and C-343 in ethanol. The absorption spectrum of C-343 in ethanol shows a peak centered at 439 nm. C-343 does not dissolve in heptane but can be dissolved in a TiO_2 NC/heptane solution because of adsorption on NCs. The absorption spectrum of the TiO_2/C-343 heptane solution exhibits a peak from adsorbed C-343 at 442 nm in addition to the strong absorption of TiO_2 below 360 nm.

The inset of Figure 6 shows a comparison of UV−visible absorption spectra of C-343-sensitized TiO_2 and ZrO_2 NCs in heptane. The absorption spectrum of C-343 adsorbed on TiO_2 NCs is slightly broader and red-shifted by 11 nm (577 cm^{-1}) compared with that of C-343 adsorbed on ZrO_2. We attribute this spectral shift to stronger electronic coupling between the C-343 excited state and TiO_2 conduction-band states.[45] Adsorption-induced red shift has been observed for other dye molecules on semiconductors.[28,32] The binding of C-343 to TiO_2 is thought to result from the chelation of the salicylate group of the dye to a Ti(IV) atom on the surface.[46] The HOMO of C-343, at +1.0 V versus SCE,[47] falls in the band gap of TiO_2, whereas

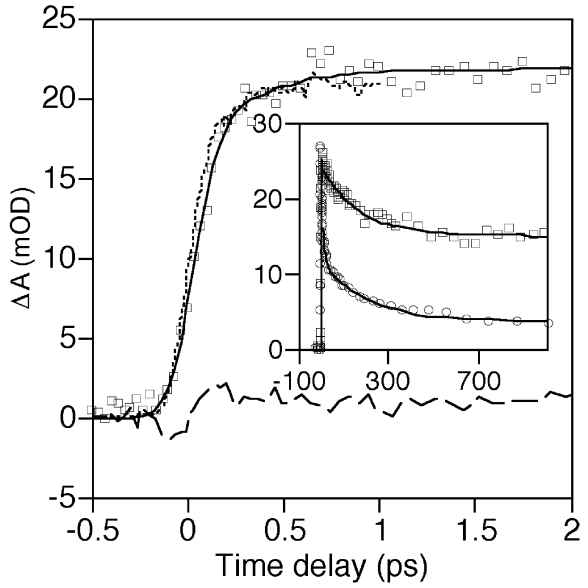

Figure 7. Transient kinetics of C-343-sensitized TiO_2 probed at 2000 cm^{-1} after 400-nm excitation. The main frame shows the early-time dynamics of C-343/TiO_2 NCs (□), a fit to the C343/TiO_2 data with a <100-fs rise time (—), the instrument response function (• • •), and the signal from unsensitized TiO_2 in heptane (− − −). The inset compares the longer-time decay dynamics of the (normalized) signal at 2000 cm^{-1} for the sensitized TiO_2 NCs (□) and NPs (○).

the LUMO, estimated to be −1.4 V versus SCE,[46,47] is above the conduction-band edge. Mixing between the LUMO (π^* orbital) of C-343 and the 3d orbitals of Ti^{4+}, which make up the lower part of the TiO_2 conduction band,[48] lowers the excited-state energies of C-343 and results in the spectral shift.[45] In contrast, the electronic coupling between C-343 and the ZrO_2 conduction band is much weaker, presumably because of the much higher conduction-band position in ZrO_2. The magnitude of the adsorption-induced peak shift of C-343 compared to that of free dyes cannot be directly determined because of the limited solubility of dyes in heptane. The absorption spectra of C-343 on TiO_2 and ZrO_2 NPs are identical (results not shown), suggesting very similar electronic coupling in those systems.

Ultrafast electron transfer was also investigated in these samples. Figure 7 shows the transient IR signal of C-343-sensitized TiO_2 NCs at 2010 cm^{-1} after excitation at 400 nm. An unsensitized TiO_2/heptane solution showed a small signal (<2 mOD), which has been subtracted from the raw C-343/TiO_2 trace, giving the trace shown in Figure 7. This signal is attributed to injected electrons in TiO_2. The dashed line indicates the instrument response time measured in a thin silicon wafer, where 400-nm excitation leads to instantaneous formation of electrons. The electron-injection time in C-343/TiO_2 is essentially instrument-response limited. We estimate that injection occurs in less than 100 fs. This is similar to the injection time seen for C-343/TiO_2 NPs, where electron injection was reported to be ∼100 fs by Ghosh et al.[22] and by Rehm et al.[49] These indicate very fast electron injection from C-343 to both TiO_2 NC and NP.

The inset to Figure 7 shows the decay of the IR transient signal extending to 1-ns delay. For comparison, the C-343/TiO_2 NP trace is reproduced from ref 22 and normalized. The C-343/TiO_2 NC data was fit using two exponential decay components with time constants (and amplitudes) of 180 ps (37%) and ≫1 ns (63%). The decay is much slower than that for the C-343-sensitized TiO_2 NPs, which is characterized by multiexponential decays with time constants ranging from 150 fs to ≫1 ns.[22]

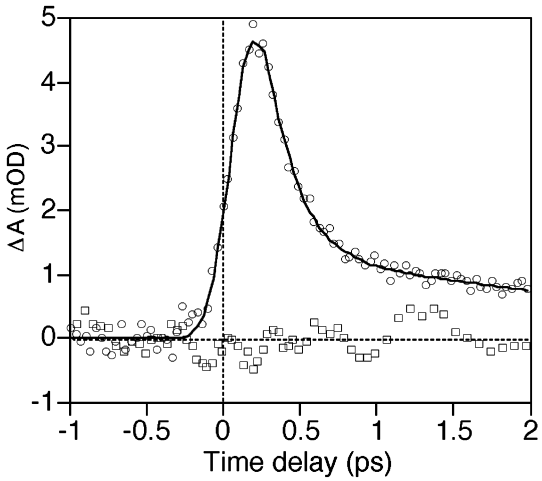

Figure 8. Transient data probing at 2000 cm^{-1} for C-343-sensitized ZrO_2 NCs (□) and NPs (○). The NC sample showed no signal, but the NP sample exhibited an instrument-limited rise and fast decay.

Both C-343-sensitized TiO_2 NCs and NPs showed indistinguishable ultrafast electron-injection times. In both cases, the charge-transfer time was 100 fs or faster. Therefore, the ability to resolve differences may be limited by the time resolution of the present experiment. To study the effect of the nanoparticle preparation on the initial electron-injection process, C-343-sensitized ZrO_2 was studied.

Electron transfer from photoexcited C-343 to the ZrO_2 conduction-band states, at about 1 eV higher than that of TiO_2,[46,47,50] should be energetically unfavorable. Kinetic traces for C-343/ZrO_2 NC and NP probing at 2000 cm^{-1} are shown in Figure 8. The small background signal observed in unsensitized ZrO_2 solution has been subtracted to give the plotted C-343/ZrO_2 traces. C-343/ZrO_2 NC showed no discernible electron-injection signal. In contrast, the C-343-sensitized ZrO_2 NPs show IR absorption signals, indicating the presence of injected electrons in ZrO_2. The absorption signal has a <100-fs rise, similar to that for C-343 on TiO_2, indicating a fast electron injection from the C-343 excited state to ZrO_2 NPs. However, the signal decays rapidly, with time constants of 180 fs and ~3 ps. This result suggests that electron injection occurs from C-343 to ZrO_2 NPs but not to ZrO_2 NCs. The nature of the electron-accepting state and the reason for the fast injection and possible back transfer will be discussed below.

To extend the comparison of electron-injection dynamics to nanocrystalline thin films, we also investigated the injection dynamics of C-343-sensitized TiO_2 and ZrO_2 nanocrystalline thin films. Shown in Figure 9 is a comparison of transient absorption signals in C-343-sensitized TiO_2 and ZrO_2 thin films in a pH 2 solution. The rise time of the electron signal in TiO_2 is instrument-response limited, suggesting a <100-fs injection time. Under the same experimental conditions (similar sample OD and same excitation power), no noticeable electron signals were observed in C-343-sensitized ZrO_2 films.

Discussion

Previous studies showed that trap states in TiO_2 nanoparticles and nanocrystalline films[51,52] affect the electron-injection,[53,54] recombination,[14−17,23,53−55] and transport kinetics.[56] In this paper, we compare ET dynamics in sensitized TiO_2 and ZrO_2 NCs and NPs. The NCs, prepared by a nonhydrolytic route in hot organic surfactants, are believed to have much better crystallinity than the NPs. One of the primary consequences of improved crystallinity is the lowered density of defect sites. An increase

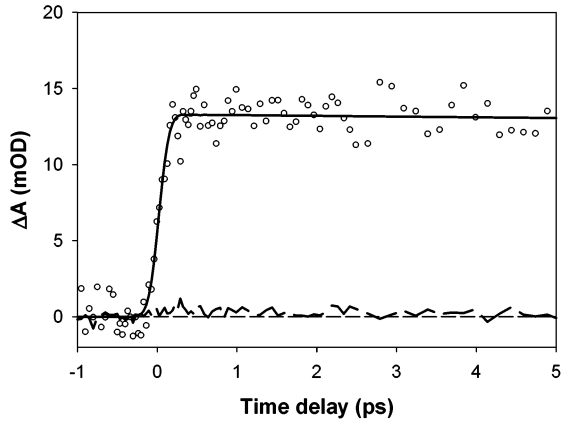

Figure 9. Transient absorption of C-343-sensitized TiO_2 (○) and ZrO_2 (− − −) nanocrystalline thin films in contact with a pH 2 aqueous solution. The solid line is a fit to the TiO_2 data with a <100-fs rise time.

in defect sites leads to a higher trap-state density below the band edge, which should significantly affect the interfacial electron-transfer dynamics, especially at energies near or below the band edge. Increasing the number of trap states within the band gap may even permit electron transfer from adsorbates whose excited-state redox potentials are lower than the conduction-band edge.

Density of Trap States. The distribution of trap states in TiO_2 NPs and NCs used for this study has not been well characterized. Two types of measurements of trap-state density distributions in other TiO_2 nanoparticles have been reported previously. The first type of experiment involved photoelectrochemical measurements of thin-film electrodes.[51,52] By measuring the optical absorption spectra of the nanocrystalline thin films under different external bias voltages, the distribution of trap states could be inferred. Rothenberger et al.[51] showed that both exponential and Gaussian distributions of trap states could be used to account for the bias-dependent absorption spectra of a TiO_2 nanocrystalline thin film. Another class of experiments used more direct techniques such as STM[57,58] and electron energy-loss spectroscopy.[59] Measurements on single rutile crystal surfaces showed a prominent peak in the trap-state density distribution 0.3[57] or 0.6 eV[59] below the conduction-band edge. Measurements of polycrystalline native TiO_2 materials revealed a much higher density of surface states and a much broader distribution compared to those of single crystals.[58] Because no direct measurement of colloidal nanoparticles in solution has been made, we assume that their trap-state distribution function resembles that of the polycrystalline TiO_2 materials[51] and can be described by an exponential decrease of the density of states below the band edge. This distribution function is often used to model electron recombination kinetics in TiO_2 thin-film electrodes.[23,55] Figure 10 shows a schematic representation of the state density in ZrO_2 and TiO_2 NPs and NCs, illustrating that NPs have a higher density of trap states extending further below the band edge.

The difference in the trap-state density in NCs and NPs is responsible for their different electron-absorption cross-section decays shown in Figure 5. The cross-section decay measured in NPs is consistent with that of a previous study of Fe(II)-$(CN)_6^{4-}$ -sensitized TiO_2 NPs,[14,15] which also showed that the electron cross section decayed by more than 50% within 1 ns. We assume that the IR absorption cross section of injected electrons depends on the density of the final states of the IR transition.[60] As the injected electrons relax from high- to low-energy states, their absorption cross section decreases. The rate

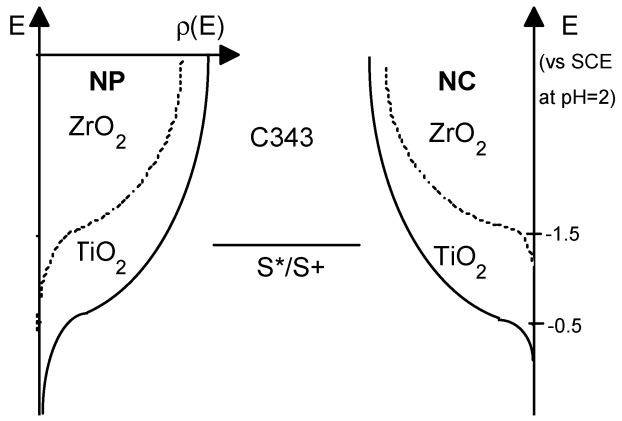

Figure 10. Schematic energetics and density-of-states diagram for electron injection in C-343-sensitized TiO_2 and ZrO_2.

of electron relaxation also depends on the trap-state distribution. In TiO_2 NCs, this relaxation will largely be the relaxation from the injected energy to the bottom of the conduction band because relaxation to the trap states is slow due to the low trap-state density. However, in NPs, the presence of more and deeper trap states allows further relaxation into the trap states and below the band edge. The electron absorption is greatly diminished in this case. Observation of faster and greater electron cross-section decay for NPs is consistent with the expected higher density of trap states for the less-crystalline nanoparticles prepared by hydrolysis.

Effect on Electron Injection. For C-343/ZrO_2, no noticeable electron injection into ZrO_2 NCs was observed. However, electron injection to the ZrO_2 NPs was observed, as indicated by the transient IR absorption signal in Figure 8. Because the excited state of C-343 likely lies near or below the band edge of ZrO_2, injection into the conduction-band state is energetically unfavorable. In this case, electron-accepting states are likely the trap states below the band edge. Therefore, electron injection from C-343 to ZrO_2 is very sensitive to the trap-state density. As illustrated in Figure 10, the ZrO_2 NCs have fewer trap states, and injection is not observed. In contrast, the larger number of trap states in the NP allows ultrafast electron injection to occur. Another possible reason for the dramatic difference in ET is the higher conduction-band edge position of ZrO_2 NCs in heptane than that of ZrO_2 NPs in pH 2 aqueous solution. The conduction-band edge of metal oxide semiconductors is known to change by -60 mV per pH unit.[61] The conduction-band edge of ZrO_2 NCs in the aprotic heptane solution may be at higher potential than that of ZrO_2 NPs in the aqueous solution of pH 2. If the distribution of trap states and the conduction-band edge have similar pH dependences, then the density of states that is involved in electron transfer from the C-343 excited state is further reduced.

These results are also consistent with the lack of electron injection from the C-343 excited state to the nanocrystalline ZrO_2 thin film in pH 2 solution, as shown in Figure 9. The film is prepared by the autoclaving and sintering of colloidal particles at high temperature. This treatment procedure forms particles of high crystallinity,[50] thus reducing the density of trap states in the material. Because both ZrO_2 thin films and colloidal NPs are in pH 2 solution, the conduction-band edges in these materials are at the same position. The lack of injection from C-343 to the ZrO_2 thin film must result from the reduction of the density of trap states. These results suggest that nanoparticle preparation can dramatically affect the electron-injection rate, especially when the redox potential of the sensitizer excited state is near or below the semiconductor conduction-band edge.

The fast decay of injected electrons in ZrO_2 may result from fast back electron transfer to C-343 or fast electron relaxation in ZrO_2. A previous study of the fluorescence of C-343 adsorbed on ZrO_2 NPs found that the fluorescence quantum yield of C-343 did not decrease as a result of adsorption.[62] One possibility that is consistent with both observations is that back ET from ZrO_2 to the C-343 excited state is efficient. Recent studies of alizarin on ZrO_2 NPs also found similar fast electron injection to trap states and fast back transfer to the S_1 excited state of the adsorbate.[53,54]

For C-343-sensitized TiO_2, ultrafast injection was observed in NCs, NPs, and thin films. The lack of an obvious difference in the injection rate can be explained in terms of smaller differences in the density of accepting semiconductor states. For NPs, a higher density of states exists below the conduction-band edge. The C-343 excited state lies $\sim$1 eV above the conduction-band edge of TiO_2 (in pH 2 solution).[46,47] At energy levels this high above the band edge, the density of states is not significantly affected by trap-state formation, and similar state densities are expected for NCs, NPs, and thin films. It is therefore reasonable to see similar electron-injection times for all C-343/TiO_2 samples. A high density of states in TiO_2 and strong electronic coupling will lead to ultrafast electron injection in all systems, without any resolvable difference within our instrument response time.

Effect on Back Electron Transfer. For catechol/TiO_2, shown in Figure 4, a faster back ET is observed for the NP sample. In our previous study of back ET in $Fe(CN)_6$/TiO_2 NP charge-transfer complexes,[15] we observed multiexponential back ET from TiO_2 to $Fe(III)(CN)_6^{3-}$, with time constants ranging from 150 fs to $\gg$1 ns. The back ET rate showed no noticeable particle size or pump-power dependence. We hypothesize that the electrons injected into NPs are trapped rapidly near the oxidized adsorbate because of the large density of trap states. The distributions of trap-state distances and energies give rise to the multiexponential recombination kinetics. The recombination kinetics can be further complicated by the competition of electron recombination and hopping to different trap sites. Electrons are more mobile in materials with fewer trap states and can move further away from the adsorbate cation. This would lead to slower electron recombination rates in these materials if the number of injected electrons per particle is small. Under our experimental conditions, we estimated that there are fewer than three injected electrons per particle. This is a possible explanation for the slower back ET observed in TiO_2 NCs compared with that in NPs.

The observed fast recombination component is similar to that previously observed for back ET in TiO_2 colloidal NPs.[14−16,63] It is different from the back ET observed in many dye-sensitized nanocrystalline thin films, which typically occurs on microsecond to millisecond time scales.[17−21,64,65] Theoretical studies[23,55] suggest that electron recombination kinetics depend on both the electron trapping/detrapping dynamics in the nanomaterials and the rate of ET at the trap sites.[23,55] As a result, the overall recombination kinetics depend on whether the trapping/detrapping rate or the ET rate is the rate-limiting step. The slow recombination kinetics can be attributed to infrequent encounters of the electrons with the adsorbate sites[14,15,17−21,64] and to slow back ET of the electron−adsorbate pair in the Marcus inverted region.[16,65−69] These studies also found that back electron transfer from nanoporous TiO_2 thin film to molecular adsorbates can occur on picosecond to nanosecond time scales, depending critically on the experimental conditions such as pump power and external bias.[19]

The origin of the much faster recombination in catechol-sensitized NCs and NPs compared to that in dye-sensitized thin films[17−21,64,65] is still unclear. One possible reason is the different electronic coupling strengths in these systems. Electronic coupling for back ET in the catechol-sensitized nanoparticles is very strong because of the catechol-to-TiO_2 charge-transfer complexes. Weaker coupling is expected for back ET in thin films sensitized by Ru bipyridyl and porphyrin complexes.[17−21,64,65] Another possible reason is the much larger number of electron random-walk pathways in the film compared to the number in nanoparticles, thus slowing down the recombination rate in the films. A detailed comparison of back ET dynamics in film and nanoparticles may become possible if back ET for the same sensitizer on different TiO_2 materials (NPs, NCs, and thin films) can be compared.

Conclusions

TiO_2 and ZrO_2 NCs were prepared by the thermal decomposition of molecular precursors in hot surfactant solvents. X-ray diffraction patterns showed that the TiO_2 NCs had much better crystallinity than the TiO_2 NPs. Interfacial electron-transfer properties were studied on C-343 dye-sensitized TiO_2 and ZrO_2 NCs as well as on catechol-sensitized TiO_2 NCs using subpicosecond mid-IR and visible transient absorption spectroscopy. By comparing our results with the results from similar studies of nanocrystalline thin film and less-crystalline NPs prepared by hydrolysis, we investigated the effects of improved crystallinity and reduced trap states on the electron-injection and the back-electron-transfer rates.

C-343-sensitized TiO_2 NCs, NPs, and thin films showed very fast electron injection. Ultrafast electron injection was observed from C-343 to ZrO_2 NPs, but there was no evidence of electron transfer to ZrO_2 NCs or thin films. On the basis of the energetics of C-343 and ZrO_2, electron injection in the NPs is attributed to a sizable density of trap states below the conduction-band edge. These observations are consistent with the assertion of significantly reduced surface trap states in the NCs. The reduction of trap states is also responsible for the slower electron cross-section decay in NCs. The electron cross-section decay is only ∼10% within 1 ns for catechol-sensitized TiO_2 NCs compared with ∼60% for TiO_2 NPs. The back electron transfer from semiconductor to sensitizer is slower in catechol-sensitized TiO_2 NC than in NP. The faster back electron transfer in NPs suggests an important role for electron trapping/detrapping in the overall electron recombination process.

Acknowledgment. The work was supported in part by the National Science Foundation Career award under grant 9733796, the ACS Petroleum Research Fund, and the Emory University Research Committee. T.L is an Alfred P. Sloan Research Fellow. The TEM images were collected in the Emory University Integrated Microscopy and Microanalytical Facility. We thank Dr. T. J. Trentler and Professor V. L. Colvin for helpful discussions regarding NC synthesis.

References and Notes

(1) O'Regan, B.; Gratzel, M. *Nature (London)* **1991**, *353*, 737.

(2) Nazeeruddin, M. K.; Kay, A.; Rodicio, I.; Humphrybaker, R.; Muller, E.; Liska, P.; Vlachopoulos, N.; Gratzel, M. *J. Am. Chem. Soc.* **1993**, *115*, 6382.

(3) Bach, U.; Lupo, D.; Comte, P.; Moser, J. E.; Weissortel, F.; Salbeck, J.; Spreitzer, H.; Gratzel, M. *Nature (London)* **1998**, *395*, 583.

(4) Serpone, N. *Res. Chem. Intermed.* **1994**, *20*, 953.

(5) Fox, M. A.; Dulay, M. T. *Chem. Rev.* **1993**, *93*, 341.

(6) *Semiconductor Nanoclusters—Physical, Chemical, and Catalytic Aspects*; Kamat, P. V., Meisel, D., Eds.; Elsevier: Amsterdam, 1997; Vol. 103.

(7) Asbury, J. B.; Hao, E.; Wang, Y.; Ghosh, H. N.; Lian, T. *J. Phys. Chem. B* **2001**, *105*, 4545.

(8) Asbury, J. B.; Wang, Y. Q.; Hao, E. C.; Ghosh, H. N.; Lian, T. *Res. Chem. Intermed.* **2001**, *27*, 315.

(9) Asbury, J. B.; Hao, E.; Wang, Y.; Lian, T. *J. Phys. Chem. B* **2000**, *104*, 11957.

(10) Ghosh, H. N.; Asbury, J. B.; Lian, T. *PINSA-A: Proc. Indian Nat. Sci. Acad., Part A* **2000**, *66*, 177.

(11) Wang, Y.; Asbury, J. B.; Lian, T. *J. Phys. Chem. A* **2000**, *104*, 4291.

(12) Asbury, J. B.; Ellingson, R. J.; Ghosh, H. N.; Ferrere, S.; Nozik, A. J.; Lian, T. *J. Phys. Chem. B* **1999**, *103*, 3110.

(13) Ellingson, R. J.; Asbury, J. B.; Ferrere, S.; Ghosh, H. N.; Sprague, J. R.; Lian, T.; Nozik, A. J. *J. Phys. Chem. B* **1998**, *102*, 6455.

(14) Weng, Y.-X.; Wang, Y.-Q.; Asbury, J. B.; Ghosh, H. N.; Lian, T. *J. Phys. Chem. B* **2000**, *104*, 93.

(15) Ghosh, H. N.; Asbury, J. B.; Weng, Y.; Lian, T. *J. Phys. Chem. B* **1998**, *102*, 10208.

(16) Martini, I.; Hodak, J. H.; Hartland, G. V. *J. Phys. Chem. B* **1998**, *102*, 607.

(17) Haque, S. A.; Tachibana, Y.; Klug, D. R.; Durrant, J. R. *J. Phys. Chem. B* **1998**, *102*, 1745.

(18) Tachibana, Y.; Haque, S. A.; Mercer, I. P.; Durrant, J. R.; Klug, D. R. *J. Phys. Chem. B* **2000**, *104*, 1198.

(19) Haque, S. A.; Tachibana, Y.; Willis, R. L.; Moser, J. E.; Graetzel, M.; Klug, D. R.; Durrant, J. R. *J. Phys. Chem. B* **2000**, *104*, 538.

(20) Hasselmann, G. M.; Meyer, G. J. *J. Phys. Chem. B* **1999**, *103*, 7671.

(21) Heimer, T. A.; Heilweil, E. J.; Bignozzi, C. A.; Meyer, G. J. *J. Phys. Chem. A* **2000**, *104*, 4256.

(22) Ghosh, H. N.; Asbury, J. B.; Lian, T. *J. Phys. Chem. B* **1998**, *102*, 6482.

(23) Nelson, J.; Haque, S. A.; Klug, D. R.; Durrant, J. R. *Phys. Rev. B: Condens. Matter* **2001**, *63*, 205321/1.

(24) Tachibana, Y.; Moser, J. E.; Graetzel, M.; Klug, D. R.; Durrant, J. R. *J. Phys. Chem.* **1996**, *100*, 20056.

(25) Burfeindt, B.; Hannapel, T.; Storck, W.; Willig, F. *J. Phys. Chem.* **1996**, *100*, 16463.

(26) Hannappel, T.; Burfeindt, B.; Storck, W.; Willig, F. *J. Phys. Chem. B* **1997**, *101*, 6799.

(27) Burfeindt, B.; Ramakrishna, S.; Zimmermann, C.; Meissner, B.; Hannappel, T.; Storck, W.; Willig, F. In *Ultrafast Phenomena XI*; Elsaesser, T., Mukamel, S., Maunane, M. M., Scherer, N. F., Eds.; Springer Series in Chemical Physics; Springer: Berlin, 1998; Vol. 63, p 636.

(28) Martini, I.; Hodak, J. H.; Hartland, G. V. *J. Phys. Chem. B* **1998**, *102*, 9508.

(29) Martini, I.; Hodak, J. H.; Hartland, G. V. *J. Phys. Chem. B* **1999**, *103*, 9104.

(30) Liu, D.; Kamat, P. V.; Thomas, K. G.; Thomas, K. J.; Das, S.; George, M. V. *J. Chem. Phys.* **1997**, *106*, 6404.

(31) Liu, D.; Fessenden, R. W.; Hug, G. L.; Kamat, P. V. *J. Phys. Chem. B* **1997**, *101*, 2583.

(32) Langdon, B. T.; MacKenzie, V. J.; Asunskis, D. J.; Kelley, D. F. *J. Phys. Chem. B* **1999**, *103*, 11176.

(33) Chikan, V.; Waterland, M. R.; Huang, J. M.; Kelley, D. F. *J. Chem. Phys.* **2000**, *113*, 5448.

(34) Hasselmann, G. M.; Meyer, G. J. *Z. Phys. Chem. (Muenchen)* **1999**, *212*, 39.

(35) Kelley, C. A.; Farzad, F.; Thompson, D. W.; Stipkala, J. M.; Meyer, G. J. *Langmuir* **1999**, *15*, 7047.

(36) Bahnemann, D.; Henglein, A.; Lilie, J.; Spanhel, L. *J. Phys. Chem.* **1984**, *88*, 709.

(37) O'Regan, B.; Moser, J.; Anderson, M.; Gratzel, M. *J. Phys. Chem.* **1990**, *94*, 8720.

(38) Lawless, D.; Serpone, N.; Meisel, D. *J. Phys. Chem.* **1991**, *95*, 5166.

(39) Moser, J.; Punchihewa, S.; Infelta, P. P.; Gratzel, M. *Langmuir* **1991**, *7*, 3012.

(40) Murray, C. B.; Norris, D. J.; Bawendi, M. G. *J. Am. Chem. Soc.* **1993**, *115*, 8706.

(41) Trentler, T. J.; Denler, T. E.; Bertone, J. F.; Agrawal, A.; Colvin, V. L. *J. Am. Chem. Soc.* **1999**, *121*, 1613.

(42) Rockenberger, J.; Scher, E. C.; Alivisatos, A. P. *J. Am. Chem. Soc.* **1999**, *121*, 11595.

(43) Liu, Y.; Dadap, J. I.; Zimdars, D.; Eisenthal, K. B. *J. Phys. Chem. B* **1999**, *103*, 2480.

(44) Zaban, A.; Ferrere, S.; Gregg, B. A. *J. Phys. Chem. B* **1998**, *102*, 452.

(45) Mulliken, R. S.; Person, W. B. *Molecular Complexes*; Wiley-Interscience: New York, 1969.

(46) Moser, J. E.; Gratzel, M. *Chem. Phys.* **1993**, *176*, 493.

(47) Murakoshi, K.; Yanagida, S.; Capel, M.; Castner, J. E. W. In *Interfacial Electron-Transfer Dynamics of Photosensitized Zinc Oxide Nanoclusters;* Shalaev, V. M., Moskovits, M., Eds.; ACS Symposium Series 679; American Chemical Society: Washington, DC, 1997; p 221.

(48) Henrich, V.; Cox, P. *The Surface Science of Metal Oxides*; Cambridge University Press: Cambridge, U.K., 1996.

(49) Rehm, J. M.; McLendon, G. L.; Nagasawa, Y.; Yoshihara, K.; Moser, J.; Gratzel, M. *J. Phys. Chem.* **1996**, *100*, 9577.

(50) Hagfeldt, A.; Gratzel, M. *Chem. Rev.* **1995**, *95*, 49.

(51) Rothenberger, G.; Fitzmaurice, D.; Gratzel, M. *J. Phys. Chem.* **1992**, *96*, 5983.

(52) Boschloo, G.; Fitzmaurice, D. *J. Phys. Chem. B* **1999**, *103*, 2228.

(53) Huber, R.; Sporlein, S.; Moser, J. E.; Gratzel, M.; Wachtveitl, J. In *Ultrafast Phenomena XII*; Springer Series in Chemical Physics; Springer: Berlin, 2001; Vol. 66, p 456.

(54) Huber, R.; Sporlein, S.; Moser, J. E.; Gratzel, M.; Wachtveitl, J. *J. Phys. Chem. B* **2000**, *104*, 8995.

(55) Nelson, J. *Phys. Rev. B: Condens. Matter* **1999**, *59*, 15374.

(56) Schwarzburg, K.; Willig, F. *Appl. Phys. Lett.* **1991**, *58*, 2520.

(57) Fan, F.-R. F.; Bard, A. J. *J. Phys. Chem.* **1990**, *94*, 3761.

(58) Casillas, N.; Snyder, S.; Smyrl, W.; White, H. *J. Phys. Chem.* **1991**, *95*, 7002.

(59) Chung, Y. W.; Lo, W. J.; Somorjai, G. A. *Surf. Sci.* **1977**, *64*, 588.

(60) Pankove, J. I. *Optical Processes in Semiconductors*; Dover: New York, 1975.

(61) Lyon, L. A.; Hupp, J. T. *J. Phys. Chem. B* **1999**, *103*, 4623.

(62) Pant, D.; Levinger, N. E. *Chem. Phys. Lett.* **1998**, *292*, 200.

(63) Cherepy, N. J.; Smestad, G. P.; Gratzel, M.; Zhang, J. Z. *J. Phys. Chem.* **1997**, *101*, 9342.

(64) Bach, U.; Tachibana, Y.; Moser, J.-E.; Haque, S. A.; Durrant, J. R.; Graetzel, M.; Klug, D. R. *J. Am. Chem. Soc.* **1999**, *121*, 7445.

(65) Kuciauskas, D.; Freund, M. S.; Gray, H. B.; Winkler, J. R.; Lewis, N. S. *J. Phys. Chem. B* **2001**, *105*, 392.

(66) Dang, X.; Hupp, J. T. *J. Am. Chem. Soc.* **1999**, *121*, 8399.

(67) Yan, S. G.; Prieskorn, J. S.; Kim, Y.; Hupp, J. T. *J. Phys. Chem. B* **2000**, *104*, 10871.

(68) Yan, S. G.; Hupp, J. T. *J. Phys. Chem.* **1996**, *100*, 6867.

(69) Lu, H.; Prieskorn, J. N.; Hupp, J. T. *J. Am. Chem. Soc.* **1993**, *115*, 4927.